# In the Quest for Stable Rescuing Mutants of p53: Computational Mutagenesis of Flexible Loop L1[†]

Yongping Pan,[‡] Buyong Ma,[‡] R. Babu Venkataraghavan,[§] Arnold J. Levine,[§] and Ruth Nussinov*[,‡,||]

*Basic Research Program, SAIC−Frederick, Incorporated, Laboratory of Experimental and Computational Biology, NCI−Frederick, Frederick, Maryland 21702, Institute for Advanced Study, Einstein Drive, Princeton, New Jersey 08540, and Sackler Institute of Molecular Medicine, Department of Human Genetics and Molecular Medicine, Sackler School of Medicine, Tel Aviv University, Tel Aviv 69978, Israel*

*Received October 6, 2004; Revised Manuscript Received November 14, 2004*

ABSTRACT: p53 is a protein with marginal stability. Its transcriptional functions are often inactivated by single missense mutations, shown to be associated with half of all human cancers. Here, we aim to design stable functional p53 mutants. We target loop L1, one of the most mobile structural motifs in the p53 core domain (p53C). Specifically, we selected Ser116 in the middle of loop L1 and mutated it to 14 other amino acids. All resulting mutants were subjected to molecular dynamics simulations, revealing a wide spectrum of stabilities. Among these, mutant S116M displayed a remarkable stability, with a structural deviation comparable to that of the experimental quadruple mutant M133L/V203A/N239Y/N268D that is thermodynamically more stable than that of the wild type by 2.6 kcal/mol. Structural analysis showed that the high stability of the S116M mutant was indeed due to the preservation of the p53C loop L1 conformation and the reduction of mobility in that region. The differential stabilities conferred by the single mutations are rationalized based on the geometries and chemical properties of the side chains introduced into this site. Linearity (i.e., nonbranched), moderate size, and balanced hydrophobic and hydrophilic properties of the side chain are crucial to the stabilizing effect of the residue substitutions.

p53 tumor-suppressor protein is among the central hubs (*1*) that regulate many important cellular functions (*2*). Among these is the prevention of cancer development by inducing the transcription of genes for cell-cycle arrest or apoptosis (*3*−*5*) in response to DNA damage or to other cellular stress. Maintaining the structural integrity of the p53 protein is therefore of crucial importance to the living organism (*1*, *2*). However, p53 is known to be only marginally stable (*6*), leaving it highly susceptible to structural perturbations, such as single-point missense mutations leading to a loss of function. It is now well-documented that many missense mutations result in the inactivation of p53 and are responsible for at least half of all human cancers (*7*−*9*). The structural consequence of cancer-related missense mutations is the much lower population of the native state because of partial or complete denaturation (*10*−*13*) and an increased population of alternate conformations that differ in their DNA-binding interfaces (*14*, *15*) or in the variable regions (*16*). These observations clearly show that the stabilization of p53 is of primary importance.

p53 has three domains: the N-terminal domain, the DNA-binding core domain (p53C),[1] and the C-terminal tetramerization domain (*14*, *17*). It functions in a tetramer form (*18*). Most of the missense mutations have been mapped to the p53C (*8*). Studies of the relationships between specific mutations and their effect on protein function and between structure and function further indicate that p53C is much more sensitive to residue substitutions than the N- and C-terminal domains (*19*). Consequently, several approaches aiming at the stabilization of the p53 structure to rescue its functions have focused on p53C, including the design of small molecules or peptides that bind to it (*16*, *20*, *21*), introduction of another mutation (*22*, *23*), or design of new stable and functional mutants (*24*, *25*). The latter approach was based on molecular evolution and combined naturally occurring stabilizing mutations, yielding a functional, stable quadruple mutant (*24*). This mutant is not only functional but also structurally very similar to that of the wild type as revealed by crystallography (*25*). This highlights the importance of the maintenance of the native conformation and the feasibility of a stable mutant design. However, the nonnaturally occurring mutations have largely not yet been explored.

The major structural features of p53C have been characterized previously (*26*). The mainframe of p53C consists of two $\beta$ sheets packed against each other, with a Zn-centered region and helix H2 packed against it (Figure 1). These $\beta$ sheets serve as the p53C scaffold. Crystallography (*25*) reveals that they are essential for the overall stability because of the main-chain hydrogen bonding and the hydrophobic

[†] This work was supported by Federal funds from the National Cancer Institute, National Institutes of Health, under contract number NO1-CO-12400.

* To whom correspondence should be addressed: NCI−Frederick Building 469, Room 151, Frederick, MD 21702. Telephone: 301-846-5579. Fax: 301-846-5598. E-mail: ruthn@ncifcrf.gov.

[‡] SAIC−Frederick, Incorporated.

[§] Institute for Advanced Study.

[||] Tel Aviv University.

[1] Abbreviations: molecular dynamics, MD; p53C, p53 core domain; root-mean-square deviation, RMSD; root-mean-square fluctuation, RMSF.

10.1021/bi047845y CCC: $30.25 
Published on Web 01/11/2005

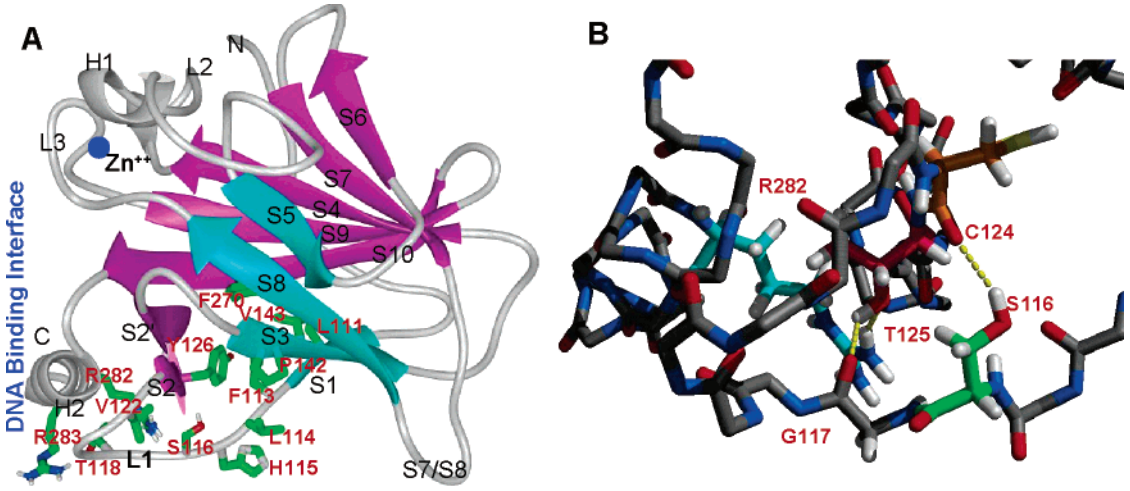


FIGURE 1: Structural features of the p53 core domain. (A) Ribbon representation of the whole core domain with some residues near loop L1 displayed. Secondary structures are labeled by black letters, and residues are labeled by red letters. (B) Atomic details of the structure near the loop L1 region showing the three hydrogen bonds near residue S116 in the crystal structure: Ser116-Cys124, Gly117-Thr125, and Thr125-Arg282.

packing among the side chains. Although the stability and structural integrity of p53C can be easily damaged by perturbations in the $\beta$ sheets as observed in the study of the temperature-sensitive missense mutations (*27*), there is little room to enhance the stability by introducing better residue packing within the already highly packed $\beta$ sheets. On the other hand, the peripheral regions including loops and turns and even the helices display higher mobility because they are loosely packed against each other or against the $\beta$ sheets (Figure 1). In addition, these mobile regions are structurally affected more than the $\beta$ sheets by missense mutations in the core region (*28*), leading to higher sensitivity to temperature and, consequently, fast unfolding. Therefore, targeting flexible regions could have direct impact on the stability of p53C.

Previous work has shown that the loop L1 region substitutions often enhanced DNA-binding affinities of p53 (*29*, *30*). For example, the S116T and the C124F/Y (*30*) mutants have higher DNA-binding affinity because of the stabilization of the loop L1 region by the introduction of the extra functional groups. On the other hand, there is only a very small number of known cancer-related mutations in this region (*7*), making loop L1 an attractive target for engineering. On the basis of these observations, we aim to systematically study the effect of mutagenesis in the loop L1 region on the local and overall stability of p53C using computations. We select residue Ser116 as the specific mutation site because of its unique location. The stability effects of 14 different mutations at this position are compared with respect to structural deviation generated in molecular dynamics (MD) simulations. Such computational experiments yield considerable insight into the physical basis of structural stabilization. On the basis of these, we identify S116M as the most stabilizing mutation.

## MATERIALS AND METHODS

MD simulations were performed using CHARMM (*31*) with the CHARMM 22 force field (*32*). The starting structures of the mutant p53C were built from the wild-type crystal structure (PDB code 1tsr) (*26*). All of the backbone and heavy atoms at the $\beta$ and $\gamma$ positions on the side chain of the replacing residue were initially superimposed on the corresponding atoms of the wild-type Ser116 in the crystal structure. The conformation of the side chain for residue 116 of the mutant was then manually adjusted to remove steric conflicts between the new side chain and the core domain. Residues such as Gln, Lys, Arg, Leu, and Met with several rotatable bonds in their side chains were kept extended. Residues Cys, Thr, Asn, and His were placed so that a hydrogen bond between their side chains and C═O group of Cys124 were initially present. The modeled mutant p53C was solvated under neutral pH in a TIP3P (*33*) water box with dimensions of about $81 \times 66 \times 63$ Å$^3$, with a minimum distance of 10 Å from any edge of the box to any protein atom, resulting in a system size of over 27 000 atoms. The positive charges in the system were balanced by adding chloride ions. The structure of the mutated residue was energetically minimized for 500 steps with the steepest decent algorithm with the backbone of the protein constrained, followed by additional 500 steps of minimization for the whole system to eliminate any other residual unfavorable interactions. The systems were then equilibrated for 20 ps with the NVT ensemble before the production simulations, which lasted for up to 5 ns with the NPT ensemble at a temperature of 300 K. During the simulations, the distances between the zinc ion and the coordinating atoms from three Cys and one His residues were constrained within ±0.1 Å of the crystal distance with the nuclear Overhauser enhancement module implemented in CHARMM. A time step of 2 fs and a nonbonded cutoff of 12 Å were used in the trajectory production. Electrostatic energies were calculated with the PME algorithm implemented in CHARMM with a switch function applied from 8 to 10 Å. Structures were saved every 2 ps for analysis.

## RESULTS AND DISCUSSION

*Selection of Mutation Site Ser116.* The most flexible region in loop L1 encompasses residues Phe113, Leu114, His115, Ser116, Gly117, and Thr118 (Figure 1). In the crystal structure, Phe113 is in tight contact with several hydrophobic residues, including Leu111, Tyr126, Val143, and Phe270 (Figure 1). Leu114 is in contact with the Pro142 side chain. His115 points away from the protein core. Ser116 interacts

Table 1: Tested Mutations at Position S116[a]

| | residue | side chain hydrogen bonding | $\beta$ branched or aromatic | biological effect |
|---|---|---|---|---|
| | Ser | × | | wild type |
| 1 | Thr | × | × | |
| 2 | Asn | × | | |
| 3 | Gln | × | | |
| 4 | Cys | × | | cancer[b] |
| 5 | His | × | × | |
| 6 | Val | | × | |
| 7 | Leu | | | |
| 8 | Met | | | |
| 9 | Pro | | | cancer[b] |
| 10 | Phe | | × | |
| 11 | Trp | | × | |
| 12 | Tyr | | × | |
| 13 | Lys | | | |
| 14 | Arg | | | |

[a] The five untested residues are Gly, Ala, Asp, Glu, and Ile. [b] These cancer related mutations were reported once each in the latest TP53 mutation database (*7*).

with Cys124 through a hydrogen bond (Figure 1). Gly117 also makes a hydrogen bond with Thr125, and its Cα hydrogens are oriented such that an introduction of a larger side chain at this position cannot directly enhance the interactions within the protein (Figure 1). Thr118 sits between two consecutive Arg residues 282 and 283, with its OH group forming a hydrogen bond with the side chain of Arg283 and its methyl group packing against the Arg282 side chain. In loop L1 region, there is also a hydrogen bond between the side chain of Thr125 and the side chain of Arg282 from helix H2 that is directly involved in DNA binding (Figure 1). Between loop L1 and the protein core, there is a large pocket with mostly hydrophobic residues residing at the bottom (Figure 1). It can be seen that residues His115, Ser116, and Gly117 of loop L1 compose the most mobile region of loop L1 because there is very little interactions between this part of the loop and the bulk protein except a hydrogen bond between Ser116 and Cys124 (Figure 1). Given the orientations of residues His115 and Gly117 in the crystal structure, it is difficult to enhance the interactions by introducing other residues at these two positions without affecting the native loop conformation, leaving Ser116 the only candidate for mutagenesis screening.

*Selection of Substituting Residues.* Among the potential mutations with 19 naturally occurring amino acids, the S116/127A mutation is known not to affect the p53 functions, while the S116/127D mutation led to the abolishment of the DNA-binding affinity because of the structural alteration (*34*). These residues (Ala and Asp) were not tested in this work. Glu has a similar property to Asp and therefore was excluded as well. Similarly, Ile was not selected because its behavior should be very similar to Val or Leu. In addition, Gly was not considered as a potential stabilizing residue because a Ser to Gly mutation at position 116 would only increase its mobility because of the loss of interactions. The remaining 14 residues, including 5 polar, 4 hydrophobic, 3 aromatic, and 2 charged, were tested for their effect on the stability of the p53C. These tested residues together with their potential to form a hydrogen bond and their geometrical features are listed in Table 1. Although a Cys or Pro substitution was reported to be potentially cancerous (*7*), the structural information from their MD trajectories can provide insight into the relationship between the structural integrity of p53C and cancer. Thus, they were also tested here.

*Control Simulations.* For MD simulations to be able to predict the stabilities of the mutant p53C with various substitutions at position 116, it is critical to ensure that the simulations are able to reproduce the difference in stability of known species. Therefore, MD simulations were first performed on the wild type and the quadruple mutant because their thermodynamic stabilities differ by 2.6 kcal/mol (*25*). Over the 5 ns trajectory, the Cα root-mean-square deviation (Cα-RMSD) for the wild-type continued to rise to reach 3 Å relative to the crystal structure, while that of the quadruple mutant was leveled at around 1.5 Å (Figure 2A). This suggests that the wild type is indeed unstable, consistent with its known marginal stability, whereas the quadruple mutant is much more stable than the wild type. Moreover, the Cα-RMSD separation between the wild type and the quadruple mutant was significant, indicating that it was responsive to stability changes and was appropriate for measuring the stability of p53C.

The stabilities of the wild type and the quadruple mutant were further compared based on the residue-based root-mean-square fluctuations (RMSFs) (Figure 3). Three observations can be made from Figure 3. First, the fluctuation profiles from the simulations were consistent with the experimental temperature factor profile (*25*). Second, the fluctuations of most residues were reduced in the quadruple mutant relative to the wild type, also consistent with the experimental data (*25*). Last, the relative extent of the reduction in residue fluctuations is similar to that revealed by X-ray data. For example, the fluctuations of residues 100−150, 180−185, 225, 240−250, and 270−280 were reduced the most, and only very little reductions in the fluctuations around residues 170 and 210 were observed. These results clearly indicate that MD simulations were able to reproduce the stability differences between the different species.

It should be noted that the fluctuations in the loop L1 region in the simulations were much larger than in the rest of the protein; these larger fluctuations were not observed in the experimental data. It is likely that crystal packing hampered the otherwise larger fluctuations of loop L1 because loop L1 is at the interface of the crystal packing, while our simulations were performed on monomers surrounded by solvent molecules. Results from p53C dimer simulations revealed lowered fluctuations in the loop L1 region (Ma et al., submitted).

*Stability of Modeled Mutants.* The 14 selected mutations at position 116 displayed a wide spectrum of effects on the stability of p53C (parts A and B of Figure 2). With the 4 hydrophobic residues (Pro, Val, Leu, and Met), the Pro and Val substitutions were destabilizing, while Leu and Met were strongly stabilizing (Figure 2A). The structural deviation for the S116P mutant was among the largest (Figure 2A), mainly because of the dramatic structural deviation in the loop L1 region (Figure 2C). Mutant S116V also suffered a large conformational change in the first 0.5 ns and then continued to deviate from the starting structure with large RMSD fluctuations (Figure 2A). The overall Cα-RMSD was well-correlated with the loop L1 structural deviation (parts A and C of Figure 2). The structural deviation for the S116L mutant was maintained at a relatively low level in the 5 ns period (Figure 2A). The average Cα-RMSD for the final 3 ns was

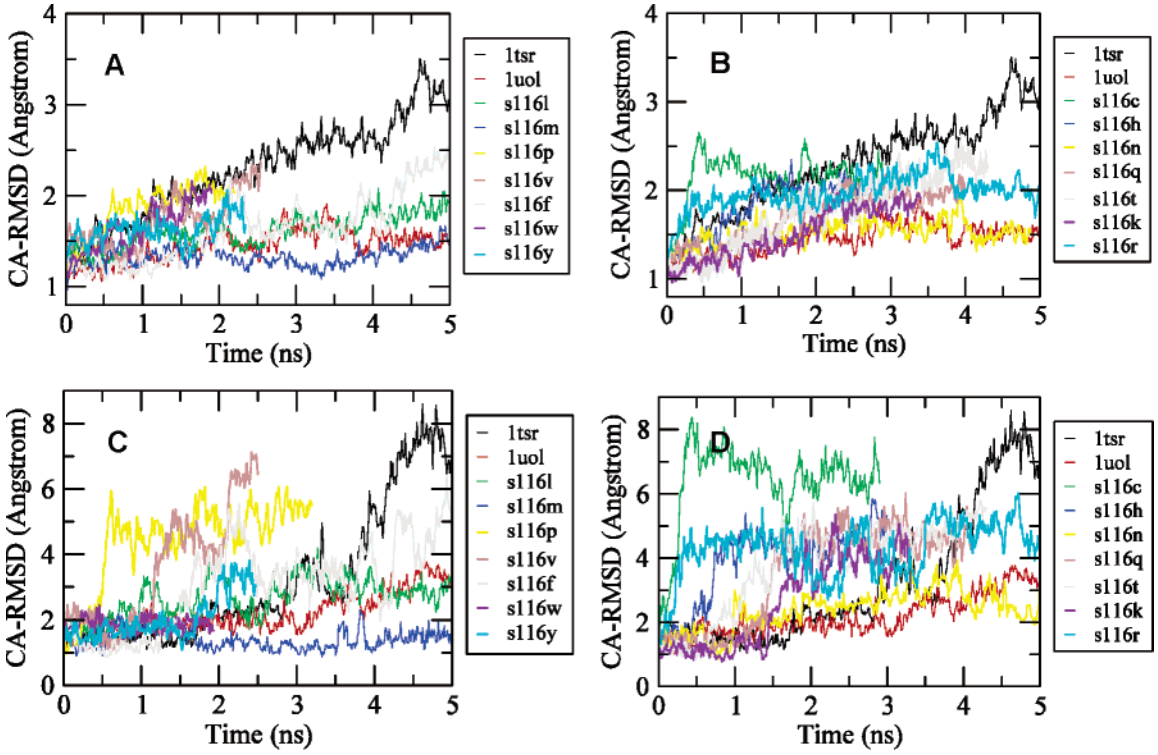


FIGURE 2: Cα RMSDs from the crystal structure. (A and B) p53 core domain. (C and D) Loop L1 (residues 113−123). The structural superimposition excludes the 3 residues at each terminus.

1.75 Å, slightly higher than that of the quadruple mutant (1.5 Å). However, loop L1 in this mutant experienced some conformational change, with an average Cα-RMSD of about 3.0 Å in the last 3 ns. Surprisingly, the S116M mutation was able to maintain the native conformation with the lowest structural deviation among all of the mutants over the 5 ns period (Figure 2A). The average RMSD for the last 3 ns was only 1.3 Å, even lower than that of the quadruple mutant. Accordingly, loop L1 in S116M only suffered a structural deviation of around 1.5 Å, lower than that of the quadruple mutant (Figure 2C).

None of the aromatic residues (Phe, Tyr, and Trp) was able to stabilize the native conformation to the extent that mutations S116L or S116M did. The Cα-RMSD of the mutant S116F was maintained at around 1.5 Å for only the first 1.5 ns. The mutant then experienced larger structural deviations during the rest of the trajectory, which were directly correlated with the disruption of the loop L1 structure (parts A and C of Figure 2). The S116Y mutant behaved similarly except that the Cα-RMSD was 1.7 Å for the first 1.5 ns, slightly larger than that of the S116F mutant (Figure 2A). This deviation is also proportional to the loop L1 conformational changes (Figure 2C). The S116W mutation caused a large overall structural change (Figure 2A). However, interestingly, the conformational change of loop L1 was moderate, with the Cα-RMSD maintained at around 2.0 Å.

From the seven polar or charged residues including Asn, Cys, Gln, His, Thr, Lys, and Arg, only the mutant S116N was able to stabilize the protein to an extent comparable to the quadruple mutant (Figure 2B). The Cα-RMSD for S116N was around 1.5 Å, although the loop L1 structural deviation was slightly higher than that of the quadruple mutant (Figure 2D). Surprisingly, the mutant S116K was the second most

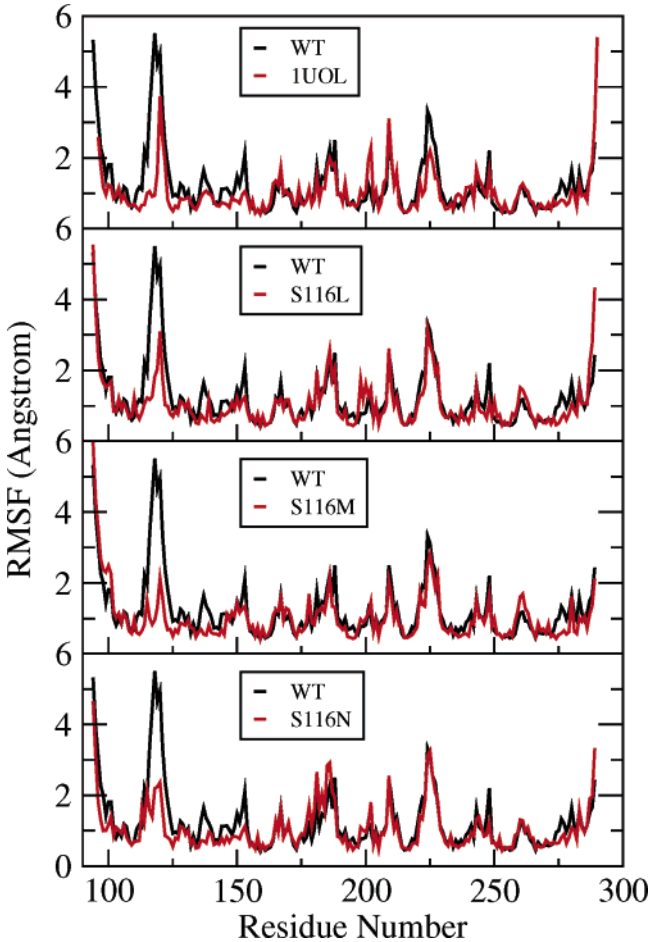


FIGURE 3: Cα RMSFs relative to the average structures of the last 3 ns of the trajectories for the quadruple mutant (PDB code 1UOL), S116L, S116M, and S116N in comparison with that of the wild type.

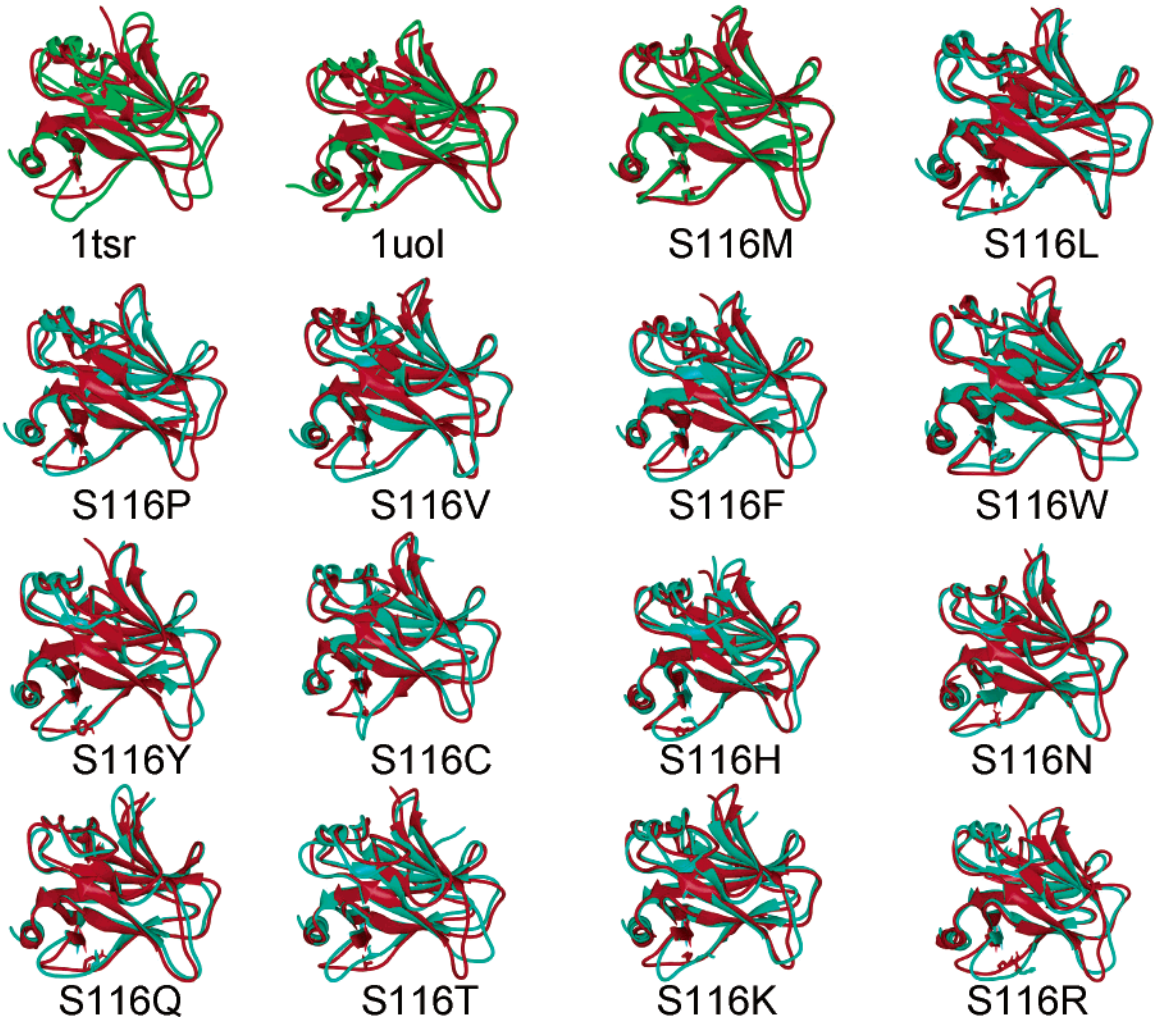


FIGURE 4: Superimposed equilibrated structures (red) before production run and average structures (green or cyan) from the last 2 ns for each of the trajectories, showing the mutational impact on the overall stability and the conformation of loop L1 and turn s7/s8. The heavy atoms of residue 116 in each of the structures are displayed.

stabilizing among the polar and charged residue substitutions (Figure 2B). The conformation of S116K was very stable for the first 1.5 ns, with an overall Cα-RMSD of 1.3 Å, among the lowest of all mutants (Figure 2B). The Cα-RMSD became larger and continued to increase afterward. The increased structural deviation was clearly related to the loop L1 movement (Figure 2D). All of the other polar mutants involved quick and large structural deviation (Figure 2B). In each case, the loop L1 region deviated most significantly (Figure 2D).

On the basis of the RMSD data from the trajectories, replacements of S116 by Met, Leu, and Asn were identified as having significant stabilizing effects on the native conformation of p53C. The trajectories of these mutants were further analyzed with respect to the individual residue fluctuations. Figure 3 compares the residue fluctuations of each of the three stable mutants with those of the wild type. Overall, the decrease in residue fluctuations was very similar among 116L, 116M, and 116N, with S116M being more stable at the mutation site (Figure 3). The most dramatic reduction of mobility in the three mutants compared with the wild type was also at the mutation site, indicating that the impact of the mutation on residue flexibility is near that site. In addition, the magnitude of the reduction in the mutation site region for all three mutants was more significant than in the quadruple mutant. These results demonstrate that the low fluctuations near residue 116 and the overall stability of the mutants were indeed the result of the residue substitution.

*Structural Basis for the Stabilization/Destabilization.* Our simulations have shown a wide spread of effects on p53C stability upon residue substitution at position 116. Detailed analysis of the interactions between the substituted residue and the bulk protein is important to understand the underlying structural basis of these effects.

*(a) Hydrogen Bond.* It would be ideal for the polar residues to have both hydrogen-bonding and favorable packing interactions with the neighboring residues. Unexpectedly, none of the polar residues was able to form a hydrogen bond without disrupting the loop conformation. The hydrogen bonds initially built between C═O of Cys124 and side chains of residue 116 in S116C, S116N, or S116T mutants only survived the equilibration phase (Figure 4). The hydrogen bond between Cys116 and Cys124 for the S116C mutant was broken shortly after the start of the production run during which the backbone constrains were removed, leaving the loop highly dynamic. Such a highly mobile region allowed a conformational adjustment, resulting in the rotation of Cys116 and the favorable interactions between Leu114 and Val122 that flank the loop L1 (Figures 1 and 4). The

hydrogen bond between the side chain NH2 of Asn116 and the C═O of Cys124 did not survive either. This residue moved toward the inner side of the loop, pointing in the opposite direction to that of the starting conformation. Such a movement led to the conformational change of the loop. However, the loop L1 change was minimal, possibly because of the small size of the residue and the absence of a branch at the $\beta$ position (Figure 4). Interestingly, no other hydrogen bond by this residue was found to contribute to the stability of this mutant. In mutant S116T, the hydrogen bond between Thr116 and Cys124 only lasted for about 0.8 ns. This hydrogen bond was more stable than that of the wild type, indicating that the extra methyl group helped the stabilization by reducing the mobility of the loop, which might help the overall stability, consistent with the experimental data (*30*). However, the overall stabilization was not significant, and both the loop L1 and the turn s7/s8 were distorted to a large extent (Figure 4).

The side chain of His116 for the S116H mutant was also initially oriented so that the hydrogen bond with Cys124 can be formed. However, the side chain of His116 rotated to the opposite direction so that the NH hydrogen-bond donor group on the side chain was far apart from residue Cys124, making the hydrogen bonding between His116 and Cys124 unlikely (Figure 4). Being polar and rigid, His116 was unable to pack well with the neighboring hydrophobic residues Leu114 and Val122. Instead, it favored polar−polar interactions with the solvent, leading to the loosening of loop L1 (Figure 4).

The S116Q mutant was unable to make a hydrogen bond with Cys124 because of geometrical mismatch. The stabilization of the S116Q mutant structure in the first 1.5 ns was due to the hydrogen bonds between the side chain C═O group of Gln116 and the two HN groups of Thr123 and Cys124, from 0.5 to 1.2 ns (data not shown). The newly formed three-centered hydrogen bond was unstable, because the backbone was forced to make a conformational change to make the donors available. As a result, the hydrogen bond between Gly117 and Thr125 (Figure 1) was also affected early in the trajectory (data not shown). Gln116 then further pulled the loop away from the bulk protein possibly because of the favorable interaction between the solvent and the polar side chain, resulting in the unfolding of loop L1 at its C-terminal end (Figure 4).

From the above observations, it seems that the intended hydrogen bonds for the polar residues were either too weak, as in the cases of S116C and S116T, posed excessive geometrical strain, as in the cases of His and Asn, or both. To investigate the importance of this hydrogen bond to the overall stability of p53C, the dynamic behavior of the hydrogen bond between Ser116 and Cys124 was followed for both the wild type and the quadruple mutant (Figure 5). As expected, this hydrogen bond was very fragile and was not formed most of the time in the wild type. In the quadruple mutant, it also displayed a high flexibility and was formed for only $^2/_3$ of the trajectory time. While it certainly contributes to the stability of p53C, the role of this hydrogen bond to the overall stability might not be critical based on these results.

*(b) Side-Chain Geometry*. The immediate dramatic change in the conformation of loop L1 in the S116P mutant resulted from the release of the backbone strain in the initial conformation. In the S116V mutant, Val116 preferred a

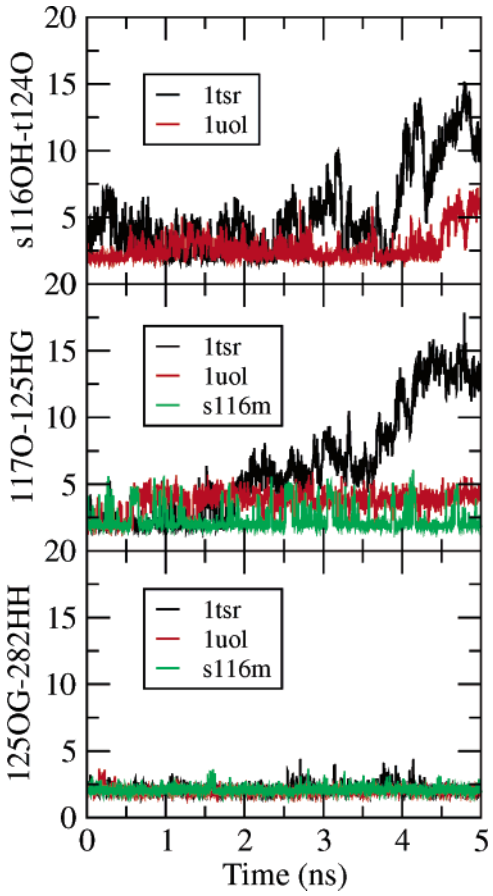


FIGURE 5: Variations of distances between 3 pairs of atoms that form hydrogen bonds in the crystal structure near residue 116. The physical locations of the residues are displayed in Figure 1B.

conformation where the two methyl groups were parallel to the loop, with each of the two methyl groups pointing toward Leu114 and Val122, respectively, to form hydrophobic interactions. However, the conformation of loop L1 changed during the first 1 ns because of the branching at the $\beta$ position of the Val side chain (Figure 2C). When the Val116 side chain pointed inward into the pocket to form hydrophobic interactions with residues Tyr126 and Phe113, loop L1 further deformed and unfolded (Figure 4). In the case of the S116L and S116M mutants, both Leu116 and Met116 made favorable interactions with their neighboring residues Leu114 and Val122. However, in S116L, the side chain of Leu116 moved further toward the inner side of the loop to form additional hydrophobic interactions with Pro142 on the other side of the loop (Figure 1), resulting in some perturbation to the loop L1 conformation (Figure 4). In the S116M mutant, the side chain of Met116 pointed straight up, almost perpendicular to the loop pocket and did not lean over to cover the pocket, which allowed a better conservation of the loop L1 conformation (Figure 4). This result indicates that the flexible linear side chain was able to adjust its conformation to avoid a steric conflict while still maintaining favorable interactions.

*(c) Side-Chain Size*. Above, we have shown that small residues such as Cys and Thr, even if they had the potential to preserve the hydrogen bond between the same residues in the wild type, have a small or even negative effect on stabilization because they cannot attain sufficient packing interactions or the hydrogen bond was too weak. On the other

hand, very large aromatic residues impacted the stability by over-restricting the motions of the nearby residues. For example, the S116F mutant was initially stabilized when the aromatic ring of Phe116 partially inserted into the pocket (Figure 4). However, such a conformation was not very stable, lasting only for 1.2 ns (parts A and C of Figure 2). Later, the pocket expanded, and the aromatic ring stretched further into the pocket to form hydrophobic interactions with residues Phe113 and Tyr126, which led to the loop disruption and conformational changes in the turn s7/s8 region (Figure 4). The S116Y mutant was stabilized in a similar manner for the first 1.5 ns, with large fluctuations in the turn s7/s8 region. However, loop L1 was again disrupted because of the penetration of the Tyr116 side chain into the pocket (Figure 4). The most significant effect caused by large-size residues can be best illustrated by the S116W mutant. With the presence of the large Trp, the available conformational space for residues neighboring Trp116 in the S116W mutant was further confined so that the loop L1 region did not suffer much conformational change (Figures 2C and 4). Instead, the motions of the protein in other regions, such as the turn s7/s8, became much higher than they were in the case of S116F and S116Y (Figure 4). Furthermore, the loop L1 conformation was preserved longer than in the S116F and S116Y mutants, because the huge side chain could not move into the pocket as easily as in Phe and Tyr (Figure 4).

*(d) Hydrophobicity*. The favorable geometry of the residues Leu and Met at position 116 allowed them to stabilize the loop and the overall structure, with loop L1 in the S116L mutant moved more than that in the S116M mutant. The Lys side chain is geometrically similar to Leu and Met, in that, it is unbranched at the $\beta$ position. The conformation of Lys116 in the S116K mutant was well-maintained in the first 1.5 ns, probably for the same reason (Figure 2D). However, because of its charged nature, the $NH_3^+$ group at the tip of the Lys116 side chain shifted away from the pocket and pointed toward the solvent (Figure 4). The difference in orientation preferences for Leu, Met, and Lys at position 116 illustrates that the balance between the hydrophilic and hydrophobic properties is important for the preservation of the loop conformation.

Figure 6 highlights the differences in the solvent-accessible surface areas (SASAs) of residue 116 in the three mutants S116K, S116L, and S116M and the differences in packing interactions measured by the VDW energy between these residues and the surrounding bulk protein. It can be seen that the SASA of the Lys116 side chain was much larger than those of Leu116 and Met116, indicating that Lys116 preferred to be more exposed to the solvent, while Met and Leu tended to anchor themselves toward the pocket. The VDW interaction energies revealed the same pattern with Lys116 making much less contact with the bulk protein than Leu116 and Met116 (Figure 6), although the interaction made by Leu116 varied because of its effect on the loop conformation.

From these results, it seems that proper geometry is important for the residue to fit into this position without deforming the loop conformation, while a balanced hydrophobic and hydrophilic property of the side chain played a major role in the maintenance of the loop and the overall stability. In general, large or $\beta$-branched residues could not stabilize the conformation because they either disrupt the conformation or impose excessive confinement on the movement of the neighboring residues. Consistent with our observations, it was recently shown that $\beta$-branched and aromatic residues have different effects on the conformations of neighboring residues as compared to other residues except Gly and Pro (*35*). On the other hand, small residues fail to stabilize p53C because of their inability to lend sufficient packing.

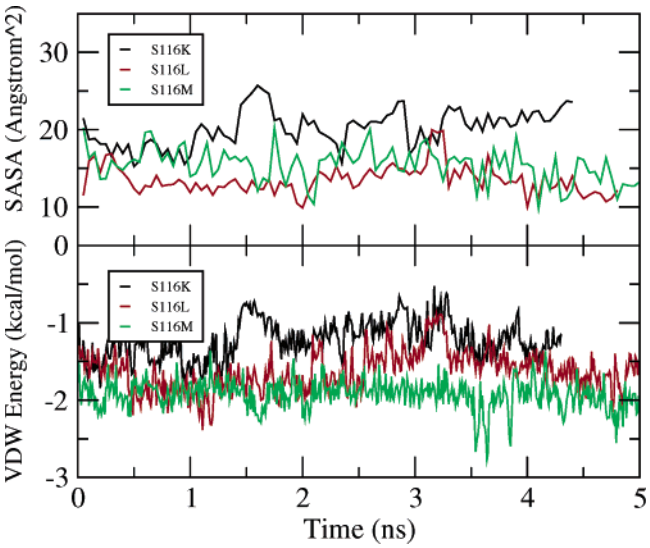


FIGURE 6: Differences between S116K, S116L, and S116M in their interactions with the environment. (A) Changes in the SASAs of residue 116. (B) Changes of the interaction energies between residue 116 and the rest of the protein. The two direct neighboring residues were excluded in the calculations of the interaction energy. Both the SASA and the interaction energy were normalized against the total number of heavy atoms on the side chain of the respective residues.

*Structural Integrity and Residue Flexibility of Mutant S116M*. We have shown that S116M is the most stable among all 14 tested mutants (parts A and B of Figure 2 and Figure 4). In addition, in this mutant, the conformations of loop L1 and the turn s7/s8 were maintained over the simulated time, remaining very close to those in the crystal structure (Figure 4). Figure 7 provides representative snapshots of the loop L1 structures from the trajectory, in atomic detail. As discussed earlier, in all other mutants, loop L1 suffered much larger deviations (Figure 4). Furthermore, the S116M mutation can stabilize loop L1 and the turn s7/s8 simultaneously, while other mutants can only preserve one of the two structural motifs at a time. For example, S116L and S116Q had small conformational changes in the s7/s8 turn, while suffering larger structural deviations in loop L1.

As mentioned earlier, there is a hydrogen bond between Gly117 and Thr125 in the wild-type crystal structure (Figure 1). This hydrogen bond was quickly broken in the wild type (Figure 5) and was short-lived in most other mutants (data not shown). Interestingly, this hydrogen bond was not even formed in the quadruple mutant most of the time (Figure 5). However, in mutant S116M, this hydrogen bond was very stable throughout the trajectory, indicating a minimum disturbance of the loop L1 region by this mutation. The hydrogen bond between residues Thr125 and Arg282, however, was stable for most of the mutants, regardless of the loop L1 conformational changes (Figure 5).

Loop flexibility is crucial to protein function. Therefore over-reduction of residue flexibility is not desirable. A $\phi$, $\psi$

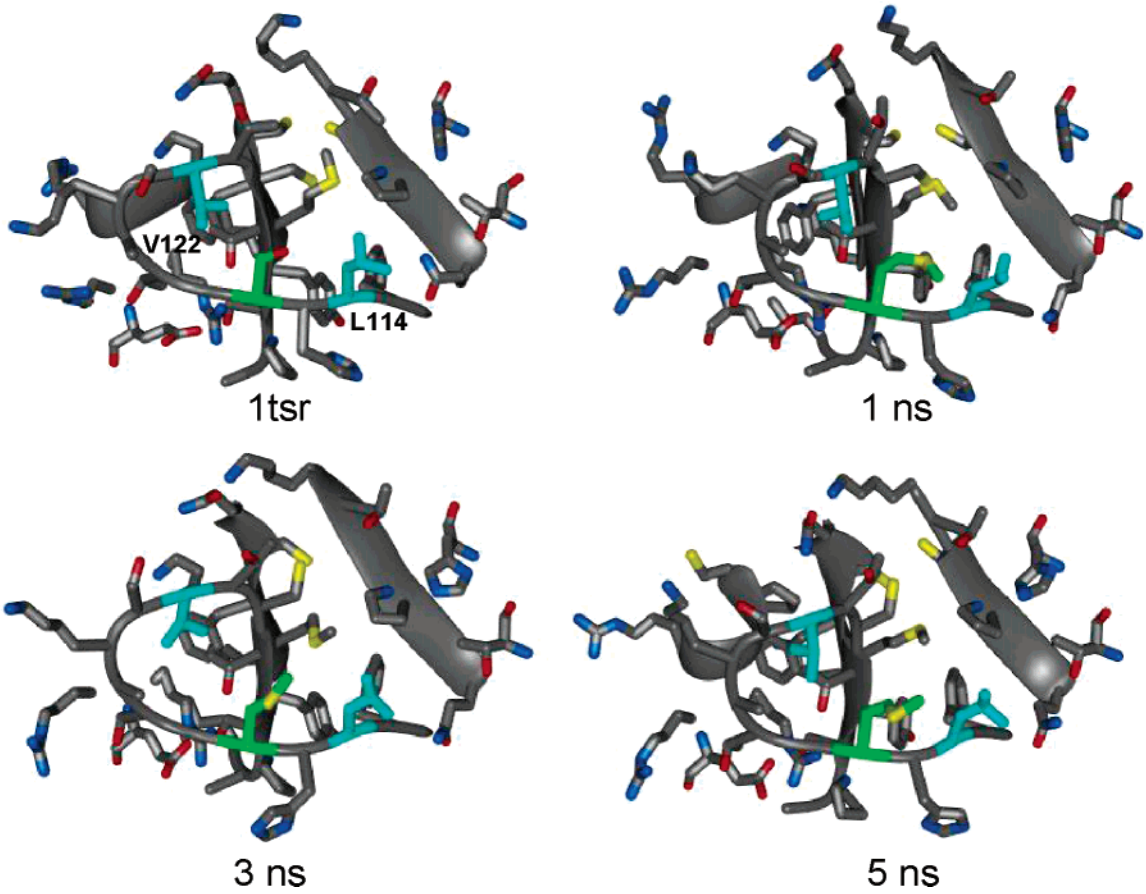


FIGURE 7: Snapshots of loop L1 structures from the S116M trajectory. All of the residues within 10 Å of residue Met116 are shown, with residue Met116 in green and Leu114 and Val122 in cyan. The loop L1 conformation from the crystal structure is also shown for comparison.

dihedral analysis shows that residues 116 and 117 in S116M actually sampled slightly larger conformational space than in the quadruple mutant (data not shown). However, the neighboring residues, including residues 120, 121, 122, and 123, sampled smaller $\phi$, $\psi$ dihedral space in S116M than in the quadruple mutant. Residue 115 sampled only $\beta$ conformations in S116M, while it sampled α-helical conformations in the quadruple mutant. However, the sampled conformational space was more diffusive in S116M than in the quadruple mutant (data not shown). Overall, these results indicate that the extent of decrease in the loop L1 flexibility by the S116M substitution was comparable to that of the functional quadruple mutant.

*Correlation between Loop L1 and Turn s7/s8.* Our simulations revealed that loop L1 changed its conformation by pulling away its C-terminal end from the helix H2 motif in most of the unstable mutants (Figure 4). This loop motion was often accompanied by the turn s7/s8 changes (Figure 4). Interestingly, the turn s7/s8, which was one of the most mobile regions revealed by the MD simulations, tended to move in the same direction as loop L1 (Figure 4), probably to avoid the close contact between these two structural motifs. Lowering the mobility of loop L1 also helped in the stabilization of the turn s7/s8, as observed in mutants S116M, S116L, and S116N (Figure 4). It was also observed that extreme confinement of residues in that position can lead to the dramatic movement in the turn s7/s8 region, as shown by the S116W mutant (Figure 2). Further understanding of such correlations in motion might yield insight into the allosteric conformational changes and its role in regulation of DNA binding, which in turn may help in the design of stable and functional p53 mutants.

*Cancer Implications of Loop L1 Structural Disruption.* Among the 14 tested mutations, S116C and S116P are potentially cancerous as discussed earlier. Interestingly, the structural deviations for both mutants increased sharply early in the trajectories. In fact, they were the two most unstable mutants of the 14 mutants based on Cα-RMSD (parts A and B of Figure 2). In both cases, the loop L1 conformation was quickly and largely disrupted, which was responsible for the overall dramatic structural change. Because residue Ser116 in the wild type is not in direct contact with the DNA in the p53C−DNA complex, such a correlation may imply that the disruption of the loop L1 conformation lead to the overall unfolding, interface disruption that affects dimer association, or conformational changes of the loop L1 residues at the C terminus that is in contact with DNA. For the latter case, it is known from the p53−DNA complex crystal structure that residues Arg280 and Lys120 bind to the DNA major groove by hydrogen bonds, defining the binding specificity (*26*, *36*). Lys120 is located at the C-terminal end of loop L1. To retain binding specificity, it is crucial to maintain residue Lys120 near its native location/conformation. The fact that both cancer-related mutants S116P and S116C had severely disrupted loop L1 conformation strongly suggests a relationship between the loop L1 conformation and DNA-binding specificity and affinity. If the stable mutant S116M, identified in the simulations, retains biological activity, it may provide direct insight into the relationship between the loop structure, stability, and function. However, the question of whether the

S116M mutant is indeed biologically viable is currently still open, requiring experimental validation.

## CONCLUSIONS

We performed computational mutagenesis on residue Ser116 in loop L1. A total of 14 different residues with various chemical and physical properties were selected as the substituting residues, and the stabilities of the corresponding mutants were tested with MD simulations. The designed mutants displayed a wide spectrum of stability effects, from extremely destabilizing, such as S116P and S116C, to highly stabilizing, such as S116L, S116M, and S116N. However, only the S116M mutation can substantially preserve the native conformation of the mobile loop L1. Detailed analysis and comparison between the properties of the residues and their effect on stability demonstrates that size, geometry, and polarity of the replacing residues were important factors in their ability to stabilize the loop L1. The correlation between the motions of loop L1 and the turn s7/s8 and possibly other regions shows that the stabilization of loop L1 might have a global effect on the protein stability. Finally, the high instability of the two cancer-related mutants is strongly supportive of the connection between the p53 function and the loop L1 conformation.

Currently, considerable efforts are being invested in approaches to stabilize p53. We hope that our work provides insight into the structural basis of the ability of different residues to stabilize p53C and suggests an efficient strategy toward the design of stable and functional mutants of p53, to be tested by experiment.

## ACKNOWLEDGMENT

We thank Drs. D. Zanuy, K. Gunasekaran, C.-J. Tsai, and H.-H. (G.) Tsai for many useful comments and suggestions. This study utilized the high-performance computational capabilities of the Biowulf PC/Linux cluster at the National Institutes of Health, Bethesda, MD (http://biowulf.nih.gov).

## REFERENCES

1. Vogelstein, B., Lane, D., and Levine, A. J. (2000) Surfing the p53 network, *Nature 408*, 307−310.
2. Bargonetti, J., and Manfredi, J. J. (2002) Multiple roles of the tumor suppressor p53, *Curr. Opin. Oncol. 14*, 86−91.
3. Kastan, M. B., Onyekwere, O., Sidransky, D., Vogelstein, B., and Craig, R. W. (1991) Participation of p53 protein in the cellular response to DNA damage, *Cancer Res. 51*, 6304−6311.
4. Polyak, K., Xia, Y., Zweier, J. L., Kinzler, K. W., and Vogelstein, B. (1997) A model for p53-induced apoptosis, *Nature 389*, 300−305.
5. Chan, T. A., Hermeking, H., Lengauer, C., Kinzler, K. W., and Vogelstein, B. (1999) 14-3-3$\sigma$ is required to prevent mitotic catastrophe after DNA damage, *Nature 401*, 616−620.
6. Bullock, A. N., Henckel, J., DeDecker, B. S., Johnson, C. M., Nikolova, P. V., Proctor, M. R., Lane, D. P., and Fersht, A. R. (1997) Thermodynamic stability of wild-type and mutant p53 core domain, *Proc. Natl. Acad. Sci. U.S.A. 94*, 14338−14342.
7. Beroud, C., and Soussi, T. (1998) p53 gene mutation: Software and database, *Nucleic Acids Res. 26*, 200−204.
8. Hainaut, P., and Hollstein, M. (2000) p53 and human cancer: The first ten thousand mutations, *Adv. Cancer Res. 77*, 81−137.
9. Hollstein, M., Rice, K., Greenblatt, M. S., Soussi, T., Fuchs, R., Sorlie, T., Hovig, E., Smith-Sorensen, B., Montesano, R., and Harris, C. C. (1994) Database of p53 gene somatic mutations in human tumors and cell lines, *Nucleic Acids Res. 22*, 3551−3555.
10. Bargonetti, J., Manfredi, J. J., Chen, X., Marshak, D. R., and Prives, C. (1993) A proteolytic fragment from the central region of p53 has marked sequence-specific DNA-binding activity when generated from wild-type but not from oncogenic mutant p53 protein, *Genes Dev. 7*, 2565−2574.
11. Hinds, P. W., Finlay, C. A., Quartin, R. S., Baker, S. J., Fearon, E. R., Vogelstein, B., and Levine, A. J. (1990) Mutant p53 DNA clones from human colon carcinomas cooperate with ras in transforming primary rat cells: A comparison of the "hot spot" mutant phenotypes, *Cell Growth Differ. 1*, 571−580.
12. Stephen, C. W., and Lane, D. P. (1992) Mutant conformation of p53. Precise epitope mapping using a filamentous phage epitope library, *J. Mol. Biol. 225*, 577−583.
13. Gannon, J. V., Greaves, R., Iggo, R., and Lane, D. P. (1990) Activating mutations in p53 produce a common conformational effect. A monoclonal antibody specific for the mutant form, *EMBO J. 9*, 1595−1602.
14. Soussi, T., and May, P. (1996) Structural aspects of the p53 protein in relation to gene evolution: A second look, *J. Mol. Biol. 260*, 623−637.
15. Soussi, T., Caron de Fromentel, C., and May, P. (1990) Structural aspects of the p53 protein in relation to gene evolution, *Oncogene 5*, 945−952.
16. Friedler, A., DeDecker, B. S., Freund, S. M., Blair, C., Rudiger, S., and Fersht, A. R. (2004) Structural distortion of p53 by the mutation R249S and its rescue by a designed peptide: Implications for "mutant conformation", *J. Mol. Biol. 336*, 187−196.
17. Soussi, T., Caron de Fromentel, C., Mechali, M., May, P., and Kress, M. (1987) Cloning and characterization of a cDNA from *Xenopus laevis* coding for a protein homologous to human and murine p53, *Oncogene 1*, 71−78.
18. Wang, P., Reed, M., Wang, Y., Mayr, G., Stenger, J. E., Anderson, M. E., Schwedes, J. F., and Tegtmeyer, P. (1994) p53 domains: Structure, oligomerization, and transformation, *Mol. Cell. Biol. 14*, 5182−5191.
19. Kato, S., Han, S. Y., Liu, W., Otsuka, K., Shibata, H., Kanamaru, R., and Ishioka, C. (2003) Understanding the function−structure and function−mutation relationships of p53 tumor suppressor protein by high-resolution missense mutation analysis, *Proc. Natl. Acad. Sci. U.S.A. 100*, 8424−8429.
20. Bykov, V. J., Issaeva, N., Shilov, A., Hultcrantz, M., Pugacheva, E., Chumakov, P., Bergman, J., Wiman, K. G., and Selivanova, G. (2002) Restoration of the tumor suppressor function to mutant p53 by a low-molecular-weight compound, *Nat. Med. 8*, 282−288.
21. Friedler, A., Hansson, L. O., Veprintsev, D. B., Freund, S. M., Rippin, T. M., Nikolova, P. V., Proctor, M. R., Rudiger, S., and Fersht, A. R. (2002) A peptide that binds and stabilizes p53 core domain: Chaperone strategy for rescue of oncogenic mutants, *Proc. Natl. Acad. Sci. U.S.A. 99*, 937−942.
22. Nikolova, P. V., Wong, K. B., DeDecker, B., Henckel, J., and Fersht, A. R. (2000) Mechanism of rescue of common p53 cancer mutations by second-site suppressor mutations, *EMBO J. 19*, 370−378.
23. Wright, J. D., Noskov, S. Y., and Lim, C. (2002) Factors governing loss and rescue of DNA binding upon single and double mutations in the p53 core domain, *Nucleic Acids Res. 30*, 1563−1574.
24. Nikolova, P. V., Henckel, J., Lane, D. P., and Fersht, A. R. (1998) Semirational design of active tumor suppressor p53 DNA binding domain with enhanced stability, *Proc. Natl. Acad. Sci. U.S.A. 95*, 14675−14680.
25. Joerger, A. C., Allen, M. D., and Fersht, A. R. (2004) Crystal structure of a superstable mutant of human p53 core domain. Insights into the mechanism of rescuing oncogenic mutations, *J. Biol. Chem. 279*, 1291−1296.
26. Cho, Y., Gorina, S., Jeffrey, P. D., and Pavletich, N. P. (1994) Crystal structure of a p53 tumor suppressor−DNA complex: Understanding tumorigenic mutations, *Science 265*, 346−355.
27. Shiraishi, K., Kato, S., Han, S. Y., Liu, W., Otsuka, K., Sakayori, M., Ishida, T., Takeda, M., Kanamaru, R., Ohuchi, N., and Ishioka, C. (2004) Isolation of temperature-sensitive p53 mutations from a comprehensive missense mutation library, *J. Biol. Chem. 279*, 348−355.
28. Ishimaru, D., Maia, L. F., Maiolino, L. M., Quesado, P. A., Lopez, P. C., Almeida, F. C., Valente, A. P., and Silva, J. L. (2003) Conversion of wild-type p53 core domain into a conformation that mimics a hot-spot mutant, *J. Mol. Biol. 333*, 443−451.
29. Saller, E., Tom, E., Brunori, M., Otter, M., Estreicher, A., Mack, D. H., and Iggo, R. (1999) Increased apoptosis induction by 121F mutant p53, *EMBO J. 18*, 4424−4437.
30. Inga, A., Monti, P., Fronza, G., Darden, T., and Resnick, M. A. (2001) p53 mutants exhibiting enhanced transcriptional activation

and altered promoter selectivity are revealed using a sensitive, yeast-based functional assay, *Oncogene 20*, 501−513.
31. Brooks, B. R., Bruccoleri, R. E., Olafson, B. D., States, D. J., Swaminathan, S., and Karplus, M. (1983) CHARMM: A program for macromolecular energy, minimization, and dynamics calculations, *J. Comput. Chem. 4*, 187−217.
32. MacKerell, A. D., Jr., Bashford, D., Jr., Bellott, M., Dunbrack, R. L., Jr., Evanseck, J. D., Field, M. J., Fischer, S., Gao, J., Guo, H., Ha, S., Joseph-McCarthy, D., Kuchnir, L., Kuczera, K., Lau, F. T. K., Mattos, C., Michnick, S., Ngo, T., Nguyen, D. T., Prodhom, B., Reiher, W. E., III, Roux, B., Schlenkrich, M., Smith, J. C., Stote, R., Straub, J., Watanabe, M., Wiorkiewicz-Kuczera, J., Yin, D., and Karplus, M. (1998) All-atom empirical potential for molecular modeling and dynamics studies of proteins, *J. Phys. Chem. B 102*, 3586−3616.
33. Jorgensen, W. L., Chandrasekhar, J., Madura, J. D., Impey, R. W., and Klein, M. L. (1983) Comparison of simple potential functions for simulating liquid water, *J. Chem. Phys. 79*, 926−935.
34. Wei, G., Liu, G., and Liu, X. (2003) Identification of two serine residues important for p53 DNA binding and protein stability, *FEBS Lett. 543*, 16−20.
35. Avbelj, F., and Baldwin, R. L. (2004) Origin of the neighboring residue effect on peptide backbone conformation, *Proc. Natl. Acad. Sci. U.S.A. 101*, 10967−10972.
36. el-Deiry, W. S., Kern, S. E., Pietenpol, J. A., Kinzler, K. W., and Vogelstein, B. (1992) Definition of a consensus binding site for p53, *Nat. Genet. 1*, 45−49.

BI047845Y